Study of the NaF-ScF3 system as a molten bath for production of Sc alloys: A combination of NMR and molecular dynamics simulations

Aydar Rakhmatullin, Kelly Machado, Didier Zanghi, Ilya Polovov, Rinat Bakirov, Konstantin Maksimtsev, Catherine Bessada

Study of the $NaF-ScF_3$ system as a molten bath for production of Sc alloys: a combination of NMR and Molecular Dynamics simulations

Aydar Rakhmatullin[1*], Kelly Machado[1], Didier Zanghi[1], Ilya B. Polovov[2], Rinat Bakirov[3], Konstantin V. Maksimtsev[2], and Catherine Bessada[1]

[1]Conditions Extrêmes et Materiaux: Haute Température et Irradiation, CEMHTI, UPR 3079 - CNRS Univ Orleans 45071 Orléans, France.

[2]Department of Rare Metals and Nanomaterials, Institute of Physics and Technology Ural Federal University, Ekaterinburg, Russia

[3]Department of Technology of mechanical engineering and instrument making, Votkinsk branch of Kalashnikov Izhevsk State Technical University, 1, Shuvalova str. 427000 Votkinsk, Russia

Corresponding author Aydar Rakhmatullin, e-mail: rakhmat@cnrs-orleans.fr

Abstract

In situ high temperature NMR spectroscopy was used to characterize the $NaF-ScF_3$ melt over a wide range of compositions. ^{19}F, ^{23}Na, and ^{45}Sc NMR spectra were acquired in $NaF-ScF_3$ melts of up to 70 mol% of ScF_3. The interpretation of all experimental results obtained *in situ* in the melt is significantly enhanced by the contribution of Molecular Dynamics (MD) calculations. A new interatomic potential for the molten $NaF-ScF_3$ system was developed by using a Polarizable Ion Model (PIM). The potential parameters were obtained by force-fitting to density functional theory (DFT) reference data. MD simulations were combined with further DFT calculations to determine NMR chemical shifts for ^{19}F, ^{23}Na, and ^{45}Sc. The agreement between the experimental NMR data and the corresponding calculated data from our applied computational protocol indicated the polymerization and network formation in the melt. Additionally, the density and the electrical conductivity in the molten state were calculated from the statistical analysis of ionic trajectories obtained through MD simulations.

Keywords: High temperature NMR, scandium fluorides, molten salts, Molecular Dynamics, DFT

1. Introduction

One of the main fields of application of scandium is the development of lightweight, high-strength aluminum alloys [1]. Scandium in aluminum-based alloys is introduced during their manufacture as an aluminum-scandium master alloy where scandium content is varied from 1.5 to 5 wt%. The structure of the Al-Sc master alloy represents a solid solution of scandium in aluminum with dispersed particles of the Al_3Sc intermetallic compound [2]. The maximal solubility of scandium in aluminum-based solid solutions does not exceed 0.8 wt% [3]. Thus, $A1_3Sc$ is formed during both initial and eutectic crystallization, and as result of decomposition of a supersaturated solid solution. This intermetallic phase, with a face centered cubic lattice, has very close geometrical parameters to the aluminum lattice that results in the unique influence of scandium on structure and properties of aluminum alloys [4].

The main manufacturers of Al-Sc master alloys use the following methods for their synthesis: direct alloying of scandium metal with aluminum, electrowinning from molten salts containing scandium salts or oxide, and aluminothermic reduction of scandium salts or Sc_2O_3 [5]. The last technique allows technological use of scandium concentrate based on $NaScF_4$ that was obtained from waste solutions arising from uranium underground leaching according to the original method [6].

Therefore, the study and comprehension of the ionic structure of the electrolyte, consisting of NaF and ScF_3, represents an important contribution to understanding the mechanism of the formation of Al_3Sc. Chemical and physical properties of this melt strongly depend on scandium speciation.

The information concerning scandium speciation in halide systems is relatively poor. Moreover, most authors have used limited number of techniques in their works. Several electrochemical studies indicated that complex Sc^{3+} ions are the only soluble scandium species in chloride and chloride-fluoride molten salts [1, 7, 8], however their structure in the melts is unknown. CsI-ScI_3 and CsCl-$ScCl_3$ mixtures were studied in detail in both molten and solid state by Raman spectroscopy over the entire composition range at temperatures up to 1000 °C [9-11]. In the molten CsI-ScI_3 system with scandium iodide mole fractions below 0.6, the presence of ScI_6^{3-} and ScI_4^- species in the equilibrium was proposed. In the CsCl-$ScCl_3$ system, a different ionic species, i.e. $ScCl_7^{4-}$, $ScCl_6^{3-}$, $Sc_2Cl_9^{3-}$, and $ScCl_4^-$, were established. A cluster-like model for the structure of pure molten $ScCl_3$ was also proposed, where fragments of scandium octahedra bridged by chlorides were terminated with scandium tetrahedra having terminal chlorides.

The aim of this contribution is to investigate the structure of molten NaF-ScF_3 binary systems by a multinuclear (^{19}F, ^{45}Sc, and ^{23}Na) *in situ* NMR spectroscopy at high temperature and by computations combining Molecular Dynamics (MD) simulations and density functional theory (DFT) calculations. To perform MD simulations over a large dynamic time interval (1 – 5 ns), a classical interaction atomic potential for NaF-ScF_3 melts has been specially developed. The interatomic potential was validated over a wide range of compositions, by computing the NMR chemical shifts of each nucleus in the framework of the density functional theory. DFT calculations were performed on configurations generated along the MD simulations without further optimization. Statistical analysis of ion trajectory from MD simulations allowed to describe accurately the structure of the melts and to establish the relation between the physicochemical and structural properties.

2. Methods and Experiments

2.1. Materials.

For the preparation of the samples, the following chemicals were used: NaF (Fluka, min. 99.9 %; dried in vacuum at 773 K for 4 h), ScF_3 (Sigma-Aldrich, 99.9 %), without further purification. All fluorides were stored in a dry box under argon atmosphere maintained below 0.3 ppm of moisture and 0.1-0.5 ppm of oxygen. Different compositions of ScF_3 and NaF were prepared by mixing and grinding the corresponding fluorides. For high temperature (HT) NMR measurements, approximately 60 mg of the mixtures were put into tightly closed high purity boron nitride crucibles to avoid any contamination by the surrounding atmosphere.

2.2.NMR spectroscopy.

The HT NMR spectra were acquired using the laser heated NMR system developed in CEMHTI Orleans [12]. The BN crucible was hermetically closed, containing the sample in powder form is placed inside the RF-coil, in the center of the cryomagnet. To insure a good homogeneous heating, the top and the bottom of the crucible are heated by a CO_2 laser (Coherent Diamond 250W), passing axially through the NMR probe. The temperature was controlled by the laser power following a preliminary calibration curve. During the experiment, the temperature was held at 10 °C above the corresponding sample melting point [13]. The melting point of the sample is clearly detected by the modification of the shape and width of the NMR line. The transition from solid to liquid state can be followed by ^{19}F NMR spectra during the heating of the sample. The desired temperature should be reached in the sample after 4-5 minutes. During the NMR experiments, the peaks do not change with time once the sample

is in the liquid state. NMR spectra of ^{19}F, ^{23}Na, and ^{45}Sc have been acquired for NaF–ScF_3 compositions ranging from 0 to 70 mol% ScF_3. It was not possible to obtain HT NMR spectra at concentrations above 70 mol%, due to the very high melting point [13]. ScF_3 has a maximum melting temperature among all simple fluorides (MF_x) T_m = 1550 ± 3 °C [14].

2.3.Molecular dynamics simulations

Molecular dynamics simulations were performed using the polarizable ion model (PIM) [15, 16]. This model uses a classical interatomic potential which is a sum of four pairwise additive interactions. The analytical expression is made up of four terms:

$$V = \sum_{i<j}\left(\frac{q^i q^j}{r^{ij}} + B^{ij}e^{-a^{ij}r^{ij}} - f_6^{ij}(r^{ij})\frac{C_6^{ij}}{(r^{ij})^6} - f_8^{ij}(r^{ij})\frac{C_8^{ij}}{(r^{ij})^8}\right) + V_{pol}$$

The first term corresponds to the electrostatic interactions. The two following terms are expressed by a Born-Huggins-Mayer type potential; they consist of an exponentially decaying term accounting for the overlap repulsion of the electronic clouds at short distances, and a term, which represents the dispersion effects. The B^{ij} and a^{ij} represent the repulsion coefficients and the C_{ij}^6 and C_{ij}^8 parameters are the dipole–dipole and dipole–quadrupole dispersion coefficients. The f_n are Tang-Toennies dispersion damping functions [17] describing the short range penetration correction to the asymptotic multipole expansion of dispersion.

Finally, the fourth term, called polarization term reflects the distortion of the electronic density in response to the electric fields due to all the other ions, which results in induced dipole on each ion [18]. This polarization term include charge-dipole and dipole-dipole interactions as well as the polarizability α, corresponding to the energy cost of deforming the charge density of the ion *i* to create the induced dipole:

$$V_{pol} = \sum_{i,j}\left[\left(q^i\mu_\alpha^j g^{ij}(r^{ij}) - q^j\mu_\alpha^i g^{ji}(r^{ij})\right)T_\alpha^{ij} - \mu_\alpha^i\mu_\beta^j T_{\alpha\beta}^{ij}\right] + \sum_i\left(\frac{1}{2\alpha^i}|\mu^i|^2\right)$$

where μ^i are induced dipoles on each ion *i*, T_α and $T_{\alpha\beta}$ are the charge–dipole and dipole–dipole interaction tensors, α^i is the polarizability of ion *i* and g^{ji} are Tang-Toennies functions.
The parameters listed in Table 1 for each atomic pair are specific of the studied system and force field used.

Their determination was made by a 'force-matching' method [19, 20] based on ab initio DFT calculations of forces, dipoles and stress tensor chosen as reference. These first-principles electronic structure calculations were performed on nine high temperature ionic configurations to cover a wide range of compositions going from 5 to 70 mol% of ScF_3. The DFT calculations were carried out by using a generalized gradient approximation (GGA) with a Perdew, Burke, and Ernzerhof (PBE) exchange-correlation functional [21] as implemented in the Vienna *Ab-Initio* Simulation Package (VASP) [22-24] with the cut-off energy (E_{cut}) fixed at 800 eV. The dispersion interactions are explicitly calculated through the use of the DFT-D3 correction [25], which gives a better representation of the interaction. The forces and dipoles on each ion were determined from the results of this calculation. The forces on each species and the stress tensors were obtained directly from each DFT calculation using the Hellmann-Feynman theorem. As for the dipoles, they were extracted by making use of the transformation of the Kohn–Sham orbitals to a Maximally Localized Wannier Function set [26]. Then the parameters in the polarizable potential were optimized by matching the dipoles, forces and stress tensors from the potential on the same ionic configuration to the *Ab-Initio* values [27]. A visual representation of the matching obtained from DFT and PIM is presented in the supporting information (Fig. 1S).

Table 1. Pair potential parameters (all of the parameters are given in atomic unit (au)). Where, B_{ij} and α_{ij} are parameters from the repulsion term; C_6^{ij} and C_8^{ij} are respectively dipole-dipole and dipole-quadrupole terms from the dispersion component between two ions at a longer range. The dipole polarizabilities of fluoride, Scandium and sodium ions obtained in this work are 8.158 au, 2.318 au and 0.847 au, respectively.

Ion pair	B_{ij}	α_{ij}	C_{ij}^6	C_{ij}^8
F^- - F^-	392.57	2.48	3.11	104.93
F^- - Sc^{3+}	51.45	1.77	4.68	33.76
F^- - Na^+	38.73	1.89	0.65	8.07
Sc^{3+} - Sc^{3+}	3.00	0.99	761.16	1454.85

Sc^{3+} - Na^{+}	0	5.22	189.72	1382.19
Na^{+} - Na^{+}	9.04	1.82	91.06	83.52

In this work, a simple cubic box corresponding to the unit cell was used with periodic boundary conditions that impose a specific symmetry on the system under study. For the MD simulations, the systems were first equilibrated using the isothermal-isobaric (NPT) ensemble for several compositions ranging from 5 to 70 mol% of ScF_3. The temperature and the average internal pressure were held at 10 °C above melting point (Table 2) and 0 GPa, respectively, by coupling the simulation cell to Nosé-Hoover thermostat chains and a barostat [28, 29]. The melting temperatures for the different compositions were extracted from the phase diagram established by Thoma and Karraker [13].

The relaxation time that sets the strength of the coupling of the system to the thermostats or to the barostat was fixed to 20 ps and the time step for integrating the equations of motion was fixed to 1 fs using the Verlet algorithm [30]. The aim of this equilibration period, whose duration was typically 200 ps, was to allow the system to reach equilibrium. The cell length was fixed to the stable average value of the NPT run. In our case, this equilibration time corresponds to the time required for the total energy of the system, the temperature and the density were calculated from length of the cell, to reach a steady state around an average value. We considered that this stability was achieved when the ratio between the average absolute deviation and the average value is less 5 %.

After the first stage of equilibration, the system was simulated for 1 ns in the canonical ensemble (NVT) by fixing the length of the cell to its average value. During this production phase, the atomic coordinates, the energies, the dipoles and the velocities of the different ions were recorded every 100 fs. The parameters of the cubic cells (compositions, number of atoms and volumes) used for simulations are provided in Table 2. The volume of the box was calculated by considering a cubic box. Using a confidence interval of 68 %, the uncertainty about the length cell was determined from the calculation of its mean value and the corresponding standard deviation on the last 100 ps of the equilibration phase.

Table 2. Molecular dynamics simulations conditions of NaF-ScF_3: compositions, number of atoms (N_{F-}, N_{Na+}, and N_{Sc3+}), volume of the cubic cell, and melting point.

mol% ScF_3	N_{F-}	N_{Na+}	N_{Sc3+}	Volume, $Å^3$	Melting point, K

0	100	100	0	3638 ±113	1268
5	115	100	5	3865 ±78	1227
10	124	94	10	3941 ±79	1186
15	138	90	16	4074 ±81	1082
20	148	85	21	4256 ±83	1123
25	120	60	20	3400 ±72	1158
28	122	56	22	3268 ±70	1135
31	124	52	24	3216 ±69	1090
33	125	50	25	3260 ±70	1004
37	126	45	27	3042 ±67	925
40	128	44	28	3061 ±67	926
46	131	38	31	3183 ±69	1175
50	132	33	33	3247 ±70	1370
56	134	29	35	3282 ±70	1483
60	143	26	39	3445 ±109	1523
70	161	20	47	3762 ±77	1665

2.4. NMR DFT computational details

The chemical shielding tensors for all atoms (^{19}F, ^{23}Na, ^{45}Sc) in the molten system NaF-ScF_3 have been calculated using the gauge including projector augmented wave (GIPAW) method [31] implemented with the NMR-CASTEP code [32, 33]. The PBE functional [21] was used for the exchange-correlation energy and the core-valence interactions were described by ultra-soft pseudopotentials (USPP) [33]. The USPP were generated during “the on the fly” generator (OTFG_USPP) included in CASTEP. The wave functions were expanded on a plane-wave

basis set with a cutoff-energy of 610 eV. The Brillouin zone was sampled using a Monkhorst–Pack grid [34] spacing of 0.05 $Å^{-1}$.

In order to take into account, the thermal agitation of the ions due to the temperature into the NMR parameters calculation, 10 snapshots were extracted every 100 ps along the MD trajectory simulated in the NVT ensemble. For each snapshot, the individual chemical shielding tensor is calculated for all the nuclei of the system. The isotropic shielding values are then averaged to give a mean value for each atomic configuration. For each composition, the isotropic chemical shielding was obtained by averaging the values obtained from the 10 snapshots [19, 35, 36]. Therefore, to convert the calculated isotropic chemical shielding into isotropic chemical shift, the definition of calibration curve relating isotropic chemical shift and shielding is necessary. For ^{45}Sc and ^{19}F the relationship reported in our previous study [37] and for ^{23}Na the relationship reported on [19] were applied.

3. Results and Discussions

3.1.HT NMR in NaF–ScF_3 melts

The NMR spectra acquired in the molten state consist in a single Lorentzian line, characteristic of a rapid exchange at the timescale of NMR between the different atomic configurations around the observed nucleus. The measured chemical shift is thus the average of the individual chemical shifts of the different species.

The ^{19}F spectra obtained in NaF–ScF_3 melts at high temperature, over the whole range of compositions are presented in Figure 1. ^{19}F chemical shifts obtained in our system ranged from -233.5 ppm to -7.9 ppm. The evolution of chemical shift was monotonous and nonlinear with composition (Fig. 2 left). This evolution is very similar to the trend already observed in the case of rare earth fluoride – alkali fluoride systems *A*F-*Re*F_3 [38, 39], LiF-ZrF_4 [40], and for the *A*F-ThF_4 [41] system (*A*= Li, Na, and K; *Re*=Y, La, Ce, Lu). This evolution is explained by the existence of three different fluoride types. At high NaF content, fluoride anions are mainly free. The signals for the terminal (non-bridging) fluorines appear in the chemical shift range from -63 to -114 ppm and the chemical shift range for the bridging fluorines is from -23 to -75 ppm [37]. Therefore, from fluorine NMR results, when ScF_3 is added, fluorine atoms start to bond with Sc atoms and to be involved in scandium based complexes $[ScF_x]_{3-x}$. For higher amounts of ScF_3, connections are formed between scandium complexes $[ScF_x]_{3-x}$ by bridging fluorides. Hence, the average coordination number around fluorine atoms tends to monotonically increase.

The ^{45}Sc chemical shift decreases linearly from 9 ppm to -2 ppm with increasing concentration of ScF_3 and it remains constant after 50 mol% (Fig. 2 right). In alkali fluoroscandate solid compounds, scandium is present in octahedral (Li_3ScF_6 [42], Na_3ScF_6 [43], $KScF_4$ [44], and $K_5Sc_3F_{14}$ [37]), seven (KSc_2F_7 [45] and $NaScF_4$ [46]) and eight ($LiScF_4$ [42]) coordinations with fluorine. The scandium chemical shifts domains are correlated with the different possible coordination state of scandium atoms. The ^{45}Sc chemical shift values for six and seven coordinated scandium environments range from -20 to 14 ppm and from -53.5 to -40 ppm, respectively [37]. Therefore, we can conclude from scandium NMR that in our melts, the average coordination number around scandium is six over the whole range of compositions.

High temperature ^{23}Na measurements were performed for the different compositions. We observe a decrease of the chemical shifts values over the whole range of ScF_3 content (Fig. 2 right). This reduction with ScF_3 addition corresponds to the increased shielding of the alkali cations. Therefore, the electronic cloud around the Na nucleus becomes more symmetric. This means that the Na–F interaction decreases with ScF_3 amount and sodium becomes free. This conclusion is important in terms of conductivity as the Na^+ ion would become the main charge carrier at high ScF_3 content.

3.2.Experimental and calculated Chemical shifts

The chemical shift is one of the most sensitive markers of the local structure. It is sensitive to the first neighbors, *i.e.* to the coordination numbers and the corresponding bond lengths. The chemical shifts, computed using the coupled MD/DFT approach, are compared with experimental data on Figure 2. The uncertainty of the calculated chemical shift was estimated to be ±5 ppm for ^{45}Sc, ±5 ppm for ^{23}Na and ±3 ppm for ^{19}F and; it is comparable with the uncertainty in NMR experimental measurements: ±2 ppm for ^{19}F, ±3 ppm for ^{45}Sc and ±1 ppm for ^{23}Na. A good agreement between the calculated and experimental shift values is observed, which indicates that the polarizable ion model used in these simulations is capable of reproducing accurately the local structure around each nucleus in the NaF-ScF_3 molten salt.

3.3.Coordination Number

The coordination numbers are obtained using the first minimum of the radial distribution function as the radius of the solvation shell to count the number of neighbors around a given ion. Figure 3 shows the proportion of each species, extracted from ion trajectory obtained by MD simulations. As mentioned above, in solid alkali fluoroscandates, the Sc^{3+} ions can usually occur in a 6-, 7-, or rarely 8-fold coordination. In the molten state, the dominant fluoroscandate

species is ScF_6^{3-} in all compositions. In contrast to the solid state, the four-fold and five-fold coordinated ScF_5^{2-} ions were found. It has to be noted that the presence of ScF_8^{5-} species was detected, but their relative concentration is very small (less than 1 %). The second species present over the whole range of concentrations is ScF_5^{2-}. Up to 40 mol%, the concentration of ScF_5^{2-} varies slightly, then it increases up to 30 mol%. It appears that ScF_7^{4-} entities starts to form at 25 mol%. The average coordination number around scandium obtained from calculations remained almost unchanged and its value was 5.8±0.1.

Figure 4 shows the fluorine environments extracted from the MD calculations. As expected, at low ScF_3 concentrations fluorine is present mainly as the free anion, whereas with an increase in ScF_3 concentration the fluorine anion takes part in the formation of anionic species containing the Sc-F bond (Sc-F$\cdots Na^+$). At around 25 mol% its concentration reaches a maximum. More than 90 % of the fluorine atoms are connected with only one scandium atom, forming the terminal fluorines. Bridging fluorides (Sc-F-Sc) appear for a concentration of ScF_3 larger than 25 mol% and it becomes the dominant fluoroscandate species for concentrations of ScF_3 exceeding 55 mol%. It should be noted that the free fluorine atoms disappear from the melt at the eutectic composition (40 mol% ScF_3) and there are only terminal and bridging fluorines. Then the polymerization process continues: 1) amount of bridging F increases rapidly which leads to the formation of bonded chain or network -F-Sc-F-Sc-; 2) three coordinated fluorine atoms start to form with the formation of bonds between the chains (Fig. 4). It is worth noting that the formation of fluorine atoms bonded with three scandium atoms is accompanied by the formation of five- and seven-fold coordinated scandium ions, whereas the concentration of six-coordinated scandium decreases. At melt compositions rich in scandium fluoride, the melt becomes fully polymerized. We can therefore deduce that the polymerization process is the origin of the variation of the density shown below.

In the case of Li- and Na-cryolites, the formation of AlF_m^{6-m} dimers bridged via common F atoms was detected by Raman, NMR spectroscopies [12, 47] and computing methods [19, 35, 48]. In contrast to these systems, in our case, formation of dimeric species was not observed.

The average coordination number around scandium obtained from calculations and NMR experiments agrees closely and it does not change with the concentration of ScF_3. Corradini *et al.* [49] compared experimental and simulation data of the molten YCl_3-$(LiCl\text{-}KCl)_{eut}$ and $LaCl_3$-$(LiCl\text{-}KCl)_{eut}$ mixtures. The average coordination number around a lanthanum ion chloride melt ranges from 6 to 8. As in our system, the yttrium coordination number remains

close to 6 across the concentration range. They propose two possible behaviors of the melt: either the cation can reduce the number of anions in its coordination shell to remain isolated, or the individual cations might begin to share anions and have overlapping shells. In other words, there is an increasing degree of corner and edge-sharing between coordination polyhedra as the YCl_3 or ScF_3 concentration increases, leading ultimately to a network structure. They show that the tendency to increase coordination number is linked to the propensity to form linkages of different types.

The average coordination number around fluorine atoms increases monotonically in case of both methods. Our calculation results are fully consistent with our earlier conclusions deduced from the NMR experimental data.

3.4. Density and electrical conductivity

Density and electrical conductivity are very important properties for industrial applications of molten salts. Such systems are rarely amenable to experimental measurements due to the high price of scandium fluoride. To the best of our knowledge, there are no data in the literature on these physical properties of NaF-ScF_3 melts. Thus, to obtain a quantitative estimation of such systems, we resorted to calculation. The good agreement shown above between calculations and experiment allows us to present computed parameters here with confidence in the accuracy of the results.

The electrical conductivity is calculated from MD simulations by taking into account the correlations of the displacements between the different species, according to the formula:

$$\sigma = \frac{e^2}{k_B T V} \lim_{t\to\infty} \frac{1}{6t} \left(\left| \sum_i q_i \delta r_i(t) \right|^2 \right)$$

where, e is the elementary charge, T is the temperature, V is the volume of the cubic cell, k_B is the Boltzmann constant, q_i is the formal charge of the atom i, and δ_{ri}(t) is the displacement of ion i in time t.

Figures 5 and 6 show the variations of the density and electrical conductivity of the NaF–ScF_3 melts with the composition. The density increases with increasing concentration of ScF_3 and after 40 mol% it remains almost constant. The conductivity shows an important decrease up to 40 mol%, and then it rapidly increases. Both physical quantities change their trend at the eutectic point due to changes of the speciation in the melt. This is consistent with the structural

analysis, which shows a decrease in the proportion of free fluoride in the melt and an increase in the involvement of fluoride in the "polymerization" process. As such, the structure of the liquids indicates an important decrease of the electrical conductivity and an increase of the density with composition in NaF–ScF_3 due to the network formation. Rollet *et al.* [51] have come to the same conclusion in the case of LiF–YF_3 system. The authors explain the decrease of the conductivity with increasing of YF_3 concentration by the network formation.

According to Figure 6, the total ionic conductivity, calculated from the molecular dynamics data, decreases when the ScF_3 content is between 5 and 40 mol% then increases again in the range 40 -70 mol%. The minimum conductivity value is reached for the eutectic concentration of 38 mol% in ScF_3. The evolution of conductivity as a function of ScF_3 content shows the same evolution as the liquidus curve. This behavior can be explained by the fact that total ionic conductivity is directly dependent on temperature and composition *x*. The total ionic conductivity (σ) can be written as a sum of individual contribution of each ion:

$$\sigma = \sum_i \rho_i |q_i| \mu_i = \sum_i \frac{N_A}{V_m} |q_i| \mu_i$$

where ρ_i, q_i and μ_i are respectively the density number, the charge and the conventional mobility of the ion of type i. The density number is given by the ratio of the Avogadro number and the molar volume: N_A/V_m. As shown in the above formula, the conductivity obeys to the ratio $\mu_i(T,x)/V_m(T,x)$ and it is given by the comparative growth, in temperature and composition, between both the molar volume V_m and ionic mobility μ_i. However, the temperature dependence of the ionic mobility is in general greater than the thermal expandability, thus, the conductivity tends to increase with temperature.

In our future work, we plan to investigate the mechanism of the Al metal dissolution in the NaF– ScF_3 melt and to analyze how different anionic species affect this process.

4. Conclusions

The local structure of scandium and fluoride ions was investigated in the molten NaF- ScF_3 system by combining HT NMR measurements and molecular dynamics simulations. From ^{45}Sc high-temperature NMR spectra an average coordination number of 6 has been determined for the scandium on all domains of composition of 5-70 mol%. The ^{19}F chemical shift evolution coincides with the existence of at least three types of fluorines: free at infinite dilution, fluorines connected with one scandium, and bridging fluorines at high ScF_3 contents.

The anionic structure was calculated for the first time for a wide range of compositions of $NaF\text{-}ScF_3$, and was in agreement with experimental results. The agreement between experimental and calculated chemical shifts for the three nuclei (^{19}F, ^{45}Sc and ^{23}Na) allows us to validate the new interatomic potential specially developed for simulating the molten binary $NaF\text{-}ScF_3$ in a wide range of composition (0–70 mol%). The validity of this polarizable ion model allows us to calculate reliable thermophysical data, such as density and electrical conductivity. Their evolutions with the ScF_3 content are consistent with the structural description of the molten $NaF\text{-}ScF_3$ systems. Analysis of computed data made it possible to identify the network formation in the melt. This work will open new perspectives for the study of structural, dynamic and thermodynamic properties of $NaF\text{-}ScF_3$ mixtures for the production of Sc alloys, for which experimental data are lacking.

Acknowledgment

This work was supported by the Ministry of Education and Science of the Russian Federation No. 02.G25.31.0210 of 27.04.2016. For the calculations, we thank the "Centre de Calcul Scientifique en region Centre" (Orleans, France). We thank also Dr. M. Salanne and Dr. M. Pitcher for useful discussions.

References:

[1] A. Kononov, E. Polyakov, High-temperature electrochemical synthesis and properties of intermetallic compounds of the Ni-Sc system Part 1. Electrochemical behaviour of Sc(III) in chloride-fluoride melts, J. Alloys Compd. 239 (1996) 103-106. https://doi.org/10.1016/0925-8388(96)02209-8.

[2] V.V. Zakharov, Kinetics of Decomposition of the Solid Solution of Scandium in Aluminum in Binary Al-Sc Alloys, Met. Sci. Heat Treat. 57 (2015) 410-414. http://dx.doi.org/10.1007/s11041-015-9897-z.

[3] S.-I. Fujikawa, M. Sugaya, H. Takei, K.-I. Hirano, Solid solubility and residual resistivity of scandium in aluminum, J. Less Common Met. 63 (1979) 87-97. https://doi.org/10.1016/0022-5088(79)90211-X.

[4] R.R. Sawtell, C.L. Jensen, Mechanical properties and microstructures of Al-Mg-Sc alloys, Metall. Trans. A 21 (1990) 421-430. http://dx.doi.org/10.1007/BF02782422.

[5] A. Suzdaltsev, A. Nikolaev, Y. Zaikov, Modern ways for obtaining Al–Sc master alloys: A review, Tsvetnye Metally 1 (2018) 69-73. http://dx.doi.org/10.17580/tsm.2018.01.09.

[6] V.N. Rychkov, E.V. Kirillov, S.V. Kirillov, G.M. Bunkov, M.S. Botalov, N.A. Poponin, A.L. Smirnov, M.A. Mashkovtsev, D.V. Smyshlyaev, Method of reprocessing of wasted

scandium-containing solutions from uranium extraction, Patent №2622201, Russian Federation, (2016).
[7] Y.P. Stangrit, V.P. Yurkinskij, Electrochemical behaviours of scandium in chloride melts, Zhurnal Prikladnoi Khimii 72 (1999) 1300-1303.
[8] Y. Castrillejo, P. Hernandez, J. Rodriguez, M. Vega, E. Barrado, Electrochemistry of scandium in the eutectic LiCl-KCl, Electrochim. Acta 71 (2012) 166-172. http://dx.doi.org/10.1016/j.electacta.2012.03.124.
[9] G.D. Zissi, G.N. Papatheodorou, Changes of vibrational modes upon melting solid $Cs_2NaScCl_6$, Cs_3ScCl_6, $Cs_3Sc_2Cl_9$ and $ScCl_3$, Chem. Phys. Lett. 308 (1999) 51-57. https://doi.org/10.1016/S0009-2614(99)00583-7.
[10] G.D. Zissi, G.N. Papatheodorou, Composition and temperature induced changes on the structure of molten $ScCl_3$-CsCl mixtures, Phys. Chem. Chem. Phys. 6 (2004) 4480-4489. http://dx.doi.org/10.1039/B408289C.
[11] M.M. Metallinou, L. Nalbandian, G.N. Papatheodorou, W. Voigt, H.H. Emons, Thermal analysis and Raman spectroscopic measurements on the scandium iodide-cesium iodide system, Inorg. Chem. 30 (1991) 4260-4264. http://dx.doi.org/10.1021/ic00022a030.
[12] V. Lacassagne, C. Bessada, P. Florian, S. Bouvet, B. Ollivier, J.-P. Coutures, D. Massiot, Structure of High-Temperature $NaF-AlF_3-Al_2O_3$ Melts: A Multinuclear NMR Study, J. Phys. Chem. B 106 (2002) 1862-1868. https://doi.org/10.1021/jp013114l.
[13] R.E. Thoma, R.H. Karraker, The Sodium Fluoride-Scandium Trifluoride System, Inorg. Chem. 5 (1966) 1933-1937. http://dx.doi.org/10.1021/ic50045a021.
[14] F.H. Spedding, B.J. Beaudry, D.C. Henderson, J. Moorman, High temperature enthalpies and related thermodynamic functions of the trifluorides of Sc, Ce, Sm, Eu, Gd, Tb, Dy, Er, Tm, and Yb, J. Chem. Phys. 60 (1974) 1578-1588. http://dx.doi.org/10.1063/1.1681233.
[15] P.A. Madden, M. Wilson, 'Covalent' effects in 'ionic' systems, Chem. Soc. Rev. 25 (1996) 339-350. http://dx.doi.org/10.1039/CS9962500339.
[16] F. Hutchinson, M. Wilson, P.A. Madden, A unified description of MCI_3 systems with a polarizable ion simulation model, Mol. Phys. 99 (2001) 811-824. https://doi.org/10.1080/00268970010022878.
[17] K.T. Tang, J.P. Toennies, An improved simple model for the van der Waals potential based on universal damping functions for the dispersion coefficients, J. Chem. Phys. 80 (1984) 3726-3741. https://doi.org/10.1063/1.447150.
[18] M. Salanne, P.A. Madden, Polarization effects in ionic solids and melts, Mol. Phys. 109 (2011) 2299-2315. http://dx.doi.org/10.1080/00268976.2011.617523.

[19] K. Machado, D. Zanghi, V. Sarou-Kanian, S. Cadars, M. Burbano, M. Salanne, C. Bessada, Study of NaF–AlF_3 Melts by Coupling Molecular Dynamics, Density Functional Theory, and NMR Measurements, J. Phys. Chem. C 121 (2017) 10289-10297. http://dx.doi.org/10.1021/acs.jpcc.7b01530.
[20] M. Salanne, C. Simon, P. Turq, P.A. Madden, Calculation of Activities of Ions in Molten Salts with Potential Application to the Pyroprocessing of Nuclear Waste, J. Phys. Chem. B 112 (2008) 1177-1183. http://dx.doi.org/10.1021/jp075299n.
[21] J.P. Perdew, K. Burke, M. Ernzerhof, Generalized Gradient Approximation Made Simple, Phys. Rev. Lett. 77 (1996) 3865-3868. http://dx.doi.org/10.1103/PhysRevLett.77.3865.
[22] G. Kresse, J. Hafner, Ab initio molecular-dynamics simulation of the liquid-metal--amorphous-semiconductor transition in germanium, Phys. Rev. B 49 (1994) 14251-14269. https://doi.org/10.1103/PhysRevB.49.14251.
[23] G. Kresse, J. Furthmüller, Efficient iterative schemes for ab initio total-energy calculations using a plane-wave basis set, Phys. Rev. B 54 (1996) 11169-11186. https://doi.org/10.1103/PhysRevB.54.11169.
[24] G. Kresse, J. Furthmüller, Efficiency of ab-initio total energy calculations for metals and semiconductors using a plane-wave basis set, Comput. Mater. Sci. 6 (1996) 15-50. https://doi.org/10.1016/0927-0256(96)00008-0.
[25] S. Grimme, J. Antony, S. Ehrlich, H. Krieg, A consistent and accurate ab initio parametrization of density functional dispersion correction (DFT-D) for the 94 elements H-Pu, J. Chem. Phys. 132 (2010) 154104. http://dx.doi.org/10.1063/1.3382344.
[26] N. Marzari, D. Vanderbilt, Maximally localized generalized Wannier functions for composite energy bands, Phys. Rev. B 56 (1997) 12847-12865. https://doi.org/10.1103/PhysRevB.56.12847.
[27] R.J. Heaton, R. Brookes, P.A. Madden, M. Salanne, C. Simon, P. Turq, A First-Principles Description of Liquid BeF_2 and Its Mixtures with LiF: 1. Potential Development and Pure BeF_2, J. Phys. Chem. B 110 (2006) 11454-11460. https://doi.org/10.1021/jp061000+.
[28] G.J. Martyna, M.L. Klein, M. Tuckerman, Nosé–Hoover chains: The canonical ensemble via continuous dynamics, J. Chem. Phys. 97 (1992) 2635-2643. https://doi.org/10.1063/1.463940.
[29] G.J. Martyna, D.J. Tobias, M.L. Klein, Constant pressure molecular dynamics algorithms, J. Chem. Phys. 101 (1994) 4177-4189. https://doi.org/10.1063/1.467468.

[30] L. Verlet, Computer "Experiments" on Classical Fluids. I. Thermodynamical Properties of Lennard-Jones Molecules, Phys. Rev. 159 (1967) 98-103. http://dx.doi.org/10.1103/PhysRev.159.98.
[31] C.J. Pickard, F. Mauri, All-electron magnetic response with pseudopotentials: NMR chemical shifts, Phys. Rev. B 63 (2001) 245101. http://dx.doi.org/10.1103/PhysRevB.63.245101.
[32] J. Clark Stewart, D. Segall Matthew, J. Pickard Chris, J. Hasnip Phil, I.J. Probert Matt, K. Refson, C. Payne Mike, First principles methods using CASTEP, Z. Kristallogr. 220 (2005) 567-570. https://doi.org/10.1524/zkri.220.5.567.65075.
[33] J.R. Yates, C.J. Pickard, F. Mauri, Calculation of NMR chemical shifts for extended systems using ultrasoft pseudopotentials, Phys. Rev. B 76 (2007) 024401. https://doi.org/10.1103/PhysRevB.76.024401.
[34] H.J. Monkhorst, J.D. Pack, Special points for Brillouin-zone integrations, Phys. Rev. B 13 (1976) 5188-5192. http://dx.doi.org/10.1103/PhysRevB.13.5188.
[35] K. Machado, D. Zanghi, M. Salanne, V. Stabrowski, C. Bessada, Anionic Structure in Molten Cryolite–Alumina Systems, J. Phys. Chem. C 122 (2018) 21807-21816. http://dx.doi.org/10.1021/acs.jpcc.8b06905.
[36] K. Machado, D. Zanghi, M. Salanne, C. Bessada, Structural, Dynamic, and Thermodynamic Study of KF–AlF3 Melts by Combining High-Temperature NMR and Molecular Dynamics Simulations, J. Phys. Chem. C (2019) in press. http://dx.doi.org/10.1021/acs.jpcc.8b11907.
[37] A. Rakhmatullin, I.B. Polovov, D. Maltsev, M. Allix, V. Volkovich, A.V. Chukin, M. Boča, C. Bessada, Combined Approach for the Structural Characterization of Alkali Fluoroscandates: Solid-State NMR, Powder X-ray Diffraction, and Density Functional Theory Calculations, Inorg. Chem. 57 (2018) 1184-1195. http://dx.doi.org/10.1021/acs.inorgchem.7b02617.
[38] C. Bessada, A.-L. Rollet, A. Rakhmatullin, I. Nuta, P. Florian, D. Massiot, In situ NMR approach of the local structure of molten materials at high temperature, C.R. Chim. 9 (2006) 374-380. http://dx.doi.org/10.1016/j.crci.2005.06.007.
[39] A.-L. Rollet, A. Rakhmatullin, C. Bessada, Local Structure Analogy of Lanthanide Fluoride Molten Salts, Int. J. Thermophys. 26 (2005) 1115-1125. http://dx.doi.org/10.1007/s10765-005-6688-6.
[40] O. Pauvert, M. Salanne, D. Zanghi, C. Simon, S. Reguer, D. Thiaudière, Y. Okamoto, H. Matsuura, C. Bessada, Ion Specific Effects on the Structure of Molten AF-ZrF_4 Systems (A^+=

Li^+, Na^+, and K^+), J. Phys. Chem. B 115 (2011) 9160-9167. http://dx.doi.org/10.1021/jp203137h.
[41] C. Bessada, A. Rakhmatullin, A.-L. Rollet, D. Zanghi, Lanthanide and actinide speciation in molten fluorides: A structural approach by NMR and EXAFS spectroscopies, J. Nucl. Mater. 360 (2007) 43-48. http://dx.doi.org/10.1016/j.jnucmat.2006.08.012.
[42] A.K. Tyagi, J. Köhler, P. Balog, J. Weber, Syntheses and structures of Li_3ScF_6 and high pressure $LiScF_4$, luminescence properties of $LiScF_4$, a new phase in the system $LiF–ScF_3$, J. Solid State Chem. 178 (2005) 2620-2625. http://dx.doi.org/10.1016/j.jssc.2005.04.038.
[43] A. Bohnsack, G. Meyer, Ternäre Halogenide vom Typ A_3MX_6. IV. [1]. Ternäre Halogenide des Scandiums mit Natrium, Na_3ScX_6 (X = F, Cl, Br): Synthese, Strukturen, Ionenleitfähigkeit, Z. Anorg. Allg. Chem. 622 (1996) 173-178. http://dx.doi.org/10.1002/zaac.19966220125.
[44] J.C. Champarnaud-Mesjard, B. Frit, $KScF_4$: A New ABX_4 Octahedral cis-trans Layered Structure., Eur. J. Solid State Inorg. Chem. 29 (1992) 161-170. https://doi.org/10.1002/chin.199221005.
[45] S. Turrell, M. Toussaint, G. Turrell, J.C. Champarnaud, G. Cuveiller, Spectroscopic studies of mixed hexa-hepta scandium fluorides, J. Mol. Struct. 143 (1986) 121-124. http://dx.doi.org/10.1016/0022-2860(86)85219-X.
[46] Y. Ai, D. Tu, W. Zheng, Y. Liu, J. Kong, P. Hu, Z. Chen, M. Huang, X. Chen, Lanthanide-doped $NaScF_4$ nanoprobes: crystal structure, optical spectroscopy and biodetection, Nanoscale 5 (2013) 6430-6438. http://dx.doi.org/10.1039/C3NR01529G.
[47] E. Robert, V. Lacassagne, C. Bessada, D. Massiot, B. Gilbert, J.P. Coutures, Study of $NaF−AlF_3$ Melts by High-Temperature ^{27}Al NMR Spectroscopy: Comparison with Results from Raman Spectroscopy, Inorg. Chem. 38 (1999) 214-217. http://dx.doi.org/10.1021/ic980677b.
[48] T. Bučko, F. Šimko, Effect of alkaline metal cations on the ionic structure of cryolite melts: Ab-initio NpT MD study, J. Chem. Phys. 148 (2018) 064501. http://dx.doi.org/10.1063/1.5017106.
[49] D. Corradini, P.A. Madden, M. Salanne, Coordination numbers and physical properties in molten salts and their mixtures, Faraday Discuss. 190 (2016) 471-486. http://dx.doi.org/10.1039/C5FD00223K.
[50] G.J. Janz, G.L. Gardner, U. Krebs, R.P.T. Tomkins, Molten Salts: Volume 4, Part 1, Fluorides and Mixtures Electrical Conductance, Density, Viscosity, and Surface Tension Data, J. Phys. Chem. Ref. Data 3 (1974) 1-115. http://dx.doi.org/10.1063/1.3253134.

[51] A.-L. Rollet, M. Salanne, H. Groult, Structural effects on the electrical conductivity of molten fluorides: Comparison between LiF–YF_3 and LiF–NaF–ZrF_4, J. Fluorine Chem. 134 (2012) 44-48. https://doi.org/10.1016/j.jfluchem.2011.04.002.

Figure Captions:

Figure 1. The ^{19}F NMR spectra of $NaF–ScF_3$ melts.

Figure 2. NMR chemical shift evolution for ^{19}F (left) and for ^{23}Na, ^{45}Sc (right) in $NaF–ScF_3$. The calculated (full markers) and experimental (empty markers) chemical shifts are shown.

Figure 3. Scandium atomic fraction of: ScF_4^- (■); ScF_5^{2-} (●); ScF_6^{3-} (▲); ScF_7^{4-} (▼), ScF_8^{5-} (♦), and average coordination (★) as a function of concentration of ScF_3 in the molten $NaF-ScF_3$ system.

Figure 4. Fluor atomic fraction of: free fluorine (■), terminal fluorine F-Sc (●), bridged fluorine Sc-F-Sc (▲), three bridged fluorine (▼), and average coordination (★) varying concentrations of ScF_3 at molten state.

Figure 5. Evolution of calculated (■) and experimental (●) [50] density as a function of mol% ScF_3 in the molten state.

Figure 6. Electrical conductivity of molten the $NaF–ScF_3$ mixtures as a function of the mol% of ScF_3 at 10 °C above melting point obtained by MD simulations.

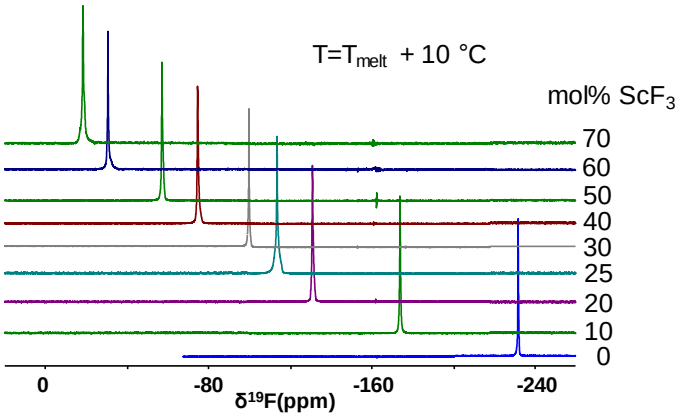

Fig.1

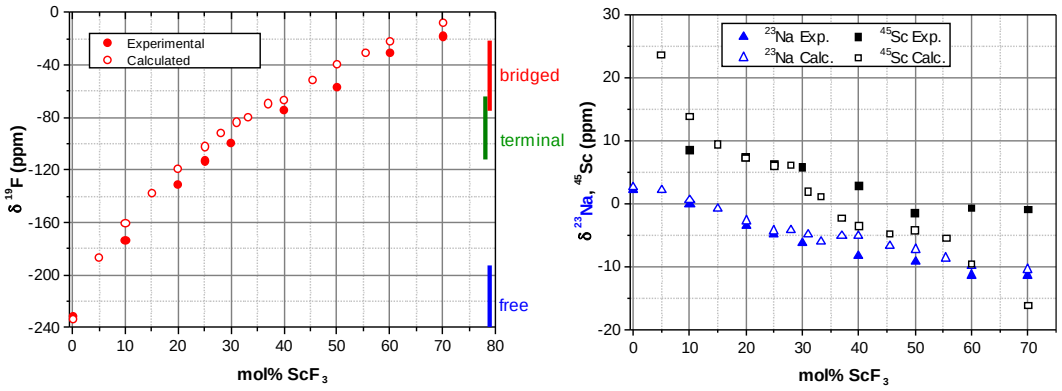

Fig.2

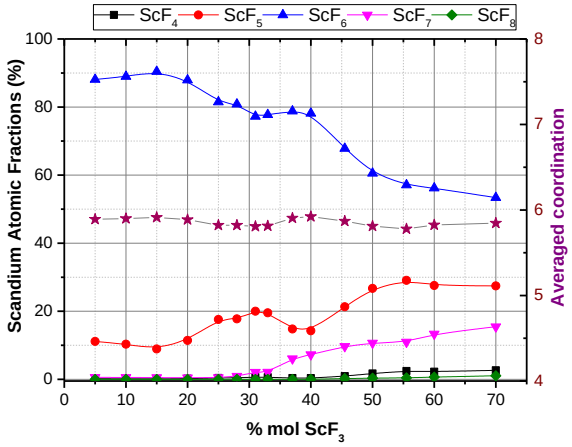

Fig.3

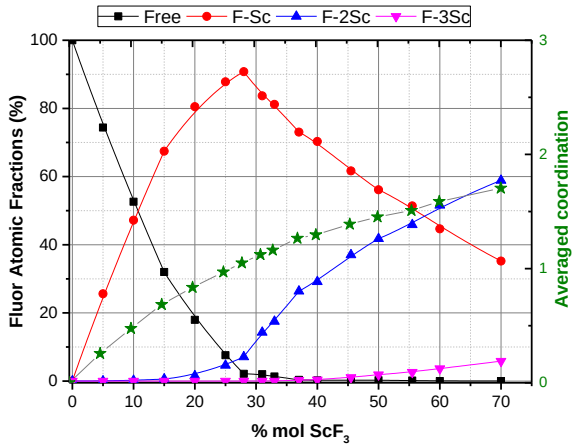

Fig.4

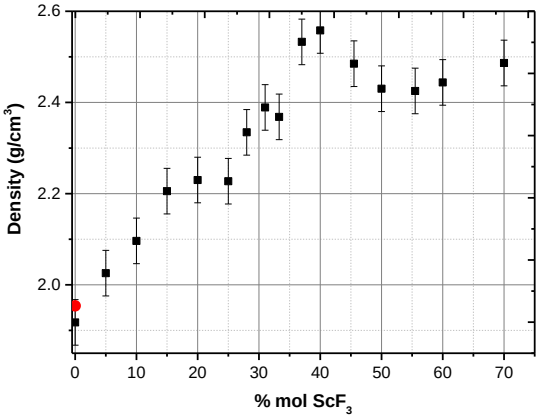

Fig.5

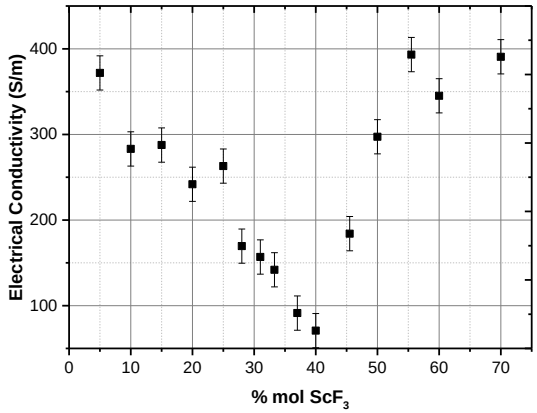

Fig.6